Enhancing the Efficiency of Self-Assembled Organic Solar Cells with the Addition of a Second Electron Donor and Graphene

Audrey Cheng

Personal

I came across an article on organic solar cells during the my time in the Garcia Research Program at Stony Brook University this past summer and was instantly fascinated by the versatility and possible uses of these devices. Imagine abundant, cheap solar cells being integrated around the world! Intrigued by the idea of using plastics to capture solar energy, I did more research into this technology. After thorough reading, I found that a significant limitation of these devices was the narrow range over which they could absorb light. I wanted to investigate enhancements to the self-assembled organic solar cell system to increase the potential of these devices. Recalling that I had studied in AP Biology how the presence of multiple types of pigments in plant leaves maximized photosynthesis, I decided to incorporate multiple donors into the solar cells after reading about similar blends in various research papers that improved device performance. I proposed adding two different kinds of light-absorbing polymers, P3HT and PCDTBT, which would capture energy at different wavelengths, to increase device efficiency.

However, the initial results weren't good at all; some devices even had lowered efficiency with the addition of P3HT. With further reading and analysis of data, I surmised that incompatibility of P3HT with the other polymers caused this decrease in electricity generation. Inspired by my previous nanomaterials research experiences, I proposed that the incorporation of graphene would improve the morphology of the active layers of the solar cells to increase solar cell performance. I thought adding graphene could increase efficiency because the high surface energy of graphene could draw the electron acceptors toward it, leading to improved morphology and increased efficiency. Graphene did improve device performance greatly, and I used various

instruments to elucidate how exactly this nanomaterial interacted with the other materials in the solar cells.

The process of conducting solar cells research has shown me that there is much uncertainty and many failures along the way. The unpredictable nature of research has taught me to be resourceful and creative when tackling obstacles. This project demonstrated that chemistry, especially nanochemistry, has much to be discovered. My project has shown me that this is the field where I can spend endless hours learning, searching, and exploring. This project has opened my eyes to the professional world of scientific research and increased my enthusiasm for science. Having seen the exciting possibilities in a career in the chemistry, I look forward to learning about more science in college and will bring what I have learned from this project to future endeavors.

Introduction

Fossil fuels provide over 70% of our current energy uses,[1] and these natural resources are rapidly depleting. As living standards increase around the world and developing countries come into their own, there will be a growing demand for energy. Even with reserves of gas and coal to supplement those of oil, our resources will eventually run out within this century. Some new reserves will be found, and more efficient devices, along with growing awareness, will lead an extended deadline, but the end of crude oil reserves is in sight. Currently, non-hydro renewable energy makes less than 8% of the world's energy supply[2] (Figure 1). Theoretically, the wind, solar, geothermal, and hydro resources could provide more energy than the world uses each day, but we currently lack the technology to harvest this energy.

Beyond concerns of insufficient supply, fossil fuels have had a devastating impact on the environment. The effects of climate change, brought largely due to the burning of fossil fuels, can be seen in the ravaged areas of world due to extreme weather, global rise in temperature, and mass

extinction of species across the world. A report by the UN[3] indicates that we are only halfway towards meeting emission pledges with the current uses. Beyond politics and the view of the public, there is an increasing need the world to transition from fossil fuels to renewable sources of energy. A key alternative to fossil resources is solar power.

Solar energy is free and easily available. Though geographical and climate conditions of solar radiation can limit its potential in some areas of the world, solar cells can be connected to battery storage and function in overcast conditions. Currently, solar energy is technologically limited by low energy conversion rates and high cost requirements for the production of solar devices.

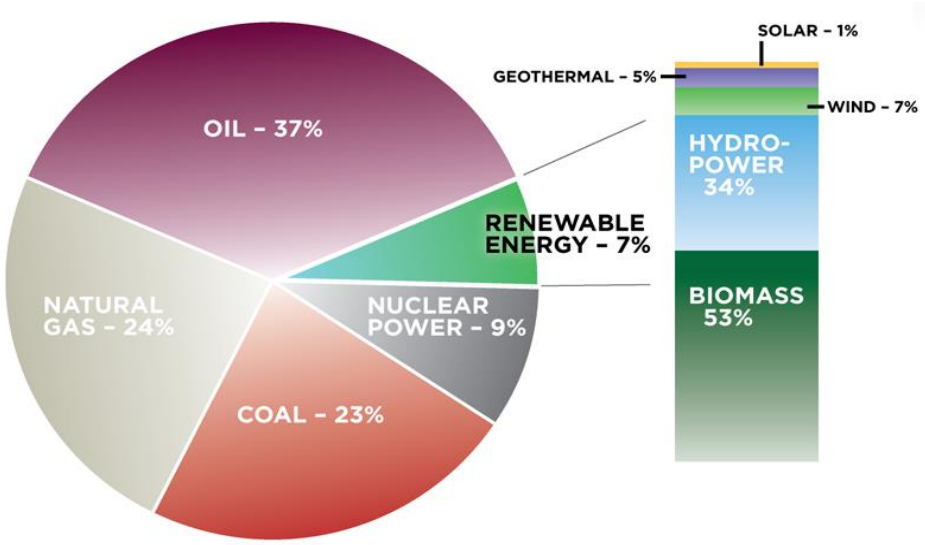

Figure 1. Breakdown of energy sources in the US from "Power in Our Hands: Renewable Energy & Fossil Fuels in the United States".

The organic solar cell is a promising alternative to current fossil fuel-based technologies and offers many unique benefits, including flexibility, semitransparency, significantly lower manufacturing costs compared to inorganic devices, and possible integration into a variety of products.[4] Organic photovoltaic (OPV) cells convert light into electrical energy by the absorption of photons, which leads to the formation of localized excitons. The excitons diffuse to interfaces

between the electron donor and electron acceptor materials, and the difference in energy between the lowest unoccupied molecular orbital (LUMO) of the donor and highest occupied molecular orbital (HOMO) of the acceptor allows charge separation to occur and drives the charge carriers towards the electrodes. This charge transport generates electrical current.[5]

Organic solar cells are characterized by their composition, fabrication processes, and purification methods. Bulk heterojunction solar cells are a type of OPVs that contain a mixture of donor and acceptor materials in the energy-generating layer, allowing for large surface areas of donor-acceptor interfaces and longer cell lifetimes.[6] Electron donors in these cells are typically photoactive polymers, while acceptors are fullerene derivatives. Highly ordered donor and acceptor domains, consisting of columnar structures, would maximize interfacial area, leading to superb charge transport and higher efficiencies, so optimization of the morphology of the active layer is critical.[4] Past research has shown that the ideal nanoscale interpenetrating network can be created by adding an immiscible polymer, such as polystyrene, into the active layer to promote lateral phase separation. [6,6]-phenyl-C_{61}-butyric acid methyl ester (PCBM), a fullerene-derivative commonly used as an electron acceptor material, has been shown preferentially segregate at the interfaces of these columns.[7]

A major limitation in organic solar cells is their relatively narrow range of absorption within the solar spectrum. The conjugated polymers used in these devices have small spectral areas of light absorption, which impede higher efficiencies. Multiple donor systems, consisting several types of electron donors that capture more photons, have been studied to overcome inherent performance limitations in these solar cells.[8] This work proposes using two donors within a self-assembled solar cell. Poly[9'-hepta-decanyl-2,7-carbazole-alt-5,5- (4',7'-di-2-thienyl-2',1',3'-benzothiadiazole) (PCDTBT), considered a next generation photoactive polymer,[9] and regio-

regular Poly(3-hexylthiophene) (P3HT), a polymer widely-studied for photovoltaic uses, were the electron donors used. PCDTBT has been shown to have better thermal and air stabilities than P3HT,[10] as well as higher efficiencies and longer lifetimes in solar cells than P3HT-based cells.[11] Previous research has shown that the introduction of large amounts of a second donor decreased efficiency, while a small fraction significantly increased efficiency.[10,11,12] It would be useful to investigate the effect of multiple donors in nanostructured organic solar cells.

Graphene, with its unique energetic band structure and full absorption range within the solar spectrum, as well as its optical transparency and remarkable mechanical properties, is a promising candidate as a superior acceptor material in organic solar cells.[13,14] The ratio of graphene to other components in the active layer has been demonstrated to be crucial to device performance. Addition of a small amount of graphene has been shown to be most effective in improving cell efficiency.[15-21] Graphene can have morphological effects on the active layer as well.[22] PCBM has been shown to gather in areas with high surface energy,[23] so it could aggregate around the graphene, which has a relatively high interface energy.[24] No work has currently been done on the incorporation of graphene into self-assembled OPVs. By exploring how the introduction of a second electron donor and graphene would affect the morphology and efficiency of nanopatterned organic solar devices, the current limitations of these solar cells can be overcome.

Materials and Methods

2.1 Preparation of Photoactive Layer Solutions:

All active layer materials were dissolved in chlorobenzene. Polystyrene (Pressure Chemical Mw 13k) was dissolved first and syringe filtered (Whatman 0.45μm). P3HT (Rieke Metals, Inc. Mw 60k) and PCDTBT (1-Material) were dissolved at 85 °C on a hot plate for 5 hours. The electron donor materials, PCBM (SES Research) and graphene (Graphene Supermarket 3nm

Graphene Nanopowder), were then added. Various concentrations of P3HT (0.5 mg/mL, 0.8 mg/mL, 1.0 mg/mL, 1.2 mg/mL) and PCBM (8 mg/mL, 12 mg/mL) were tested while the PCDTBT (4 mg/mL) and PS (2 mg/mL) concentrations were held constant. A small amount of graphene (0.1 mg/mL) was tested in one device.

2.2 Device Fabrication and Performance:

For device fabrication, indium tin oxide (ITO)-coated glass slides were polished in UV ozone for 10 minutes using a Bioforce Nanosciences UV Ozone oven. A TiO_2 solution was synthesized according to Xue et al.[25] A 30 nm thick TiO_2 layer was spun-cast (Headway Research PMW 32 spin-caster) onto each ITO glass slide at 3000 rpm for 20 seconds and then heated at 400 °C for 2 hours on a hot plate exposed to ambient air. The active layer solution was spun-cast on top of the TiO_2 layer in atmospheric conditions. The samples were then annealed in a HOTPACK Vacuum Oven at 150 °C for 10 minutes. Finally, the devices were completed by thermal evaporation to deposit an 8 nm MoO_3 film and Ag electrodes 100 nm in diameter onto the devices using Kurt J. Lesker PVD 75 vacuum deposition systems. The performance of each solar cell was tested by a 150 W solar simulator (Oriel) with an AM 1.5 G filter for solar illumination. The light intensity was calibrated to 100 mW/cm^{-2} by a calibrated thermopile detector (Oriel). Each device was measured in four different locations to ensure that the results obtained were representative of the entire solar cell.

2.3 UV-Vis Spectroscopy:

Ultraviolet-visible (UV-Vis) spectroscopy was used to analyze the absorption spectrum of the active layers. Solutions were spin-casted at 2000 rpm for 45 seconds onto methanol-cleaned ITO-coated glass slides and then scanned with a Thermo Scientific Evolution 200 UV-VIS Spectrophotometer in the visible spectrum.

2.4 Transmission Electron Microscopy:

Transmission Electron Microscopy (TEM) images were taken of samples using a Philips EM301 TEM. These images verified that self-assembled features were present within the active layer.

2.5 Construction and Characterization of Bi-layer Structures:

To explore the interactions of the polymers in the active layer, bi-layer coatings of the polymers were made. The bi-layer structures were created on 200 μm thick silicon (Si) wafers of 100 orientation (Wafer World Co.) that were cut into individual 1 cm^2 squares. The Si chips were rinsed with DI water twice to get rid of any dust or debris and then cleansed by boiling the wafers in base piranha solution, composed of ammonium hydroxide, hydrogen peroxide, and DI water in a 1:1:3 ratio, to clean off any organic contaminants and metallic ions. The wafers were boiled again in acid piranha solution, composed of sulfuric acid, hydrogen peroxide, and DI water in a 1:1:3 ratio, in order to remove any remaining impurities on the surface. The Si chips were rinsed twice in DI water and soaked in water after the cleaning process.

Solutions of PCDTBT (15 mg/mL), P3HT (15 mg/mL), and PS of Mw 13k (15 mg/mL) were made in chlorobenzene for the primary polymer thin films. Each Si wafer was dipped in a solution of 5% Hydrofluoric Acid (Fischer Scientific) for 10 seconds prior to spin-casting, changing the surface chemical composition from hydrophilic Si(OH) to hydrophobic SiO_2, to induce compatibility with the hydrophobic polymers. Four drops of each solution were placed onto a cleaned Si wafer before it was spun-cast (Headway Research PMW 32 spin-caster) at 2000 rpm for 30 seconds. The polymer thin films averaged around 80 to 90 nm in thickness when measured with an ellipsometer. The coated Si squares were then placed in covered glass containers and annealed in a HOTPACK Vacuum Oven at 150°C for 12 hours.

For the secondary polymer films, solutions of PCDTBT (5 mg/mL), P3HT (5 mg/mL), and PS of Mw 13k (5 mg/mL) were prepared in chlorobenzene. Cleaned Si wafers were placed into a Bioforce Nanoscience UV Oven for 20 minutes to oxidize their surfaces and make them effectively hydrophilic, so that the polymer thin films coated on immediately afterwards could be easily removed. Four drops of each solution were placed onto an ozone-treated Si wafer and spun-cast at 2500 rpm for 30 seconds. When measured by an ellipsometer, the polymer thin films averaged around 20 nm in thickness. The secondary thin films were each cut with a razor blade and placed slowly into a tub of DI water to remove the polymer film from the glass substrate. The free-floating 20 nm secondary film pieces were then transferred onto the primary polymer thin films. The samples were annealed for 3 days to allow the dewetting process to occur. The PCDTBT on P3HT sample did not show much phase-separation after 3 days, so it was annealed for an additional 4 days to further the process.

2.6 Atomic Force Microscopy:

The active layers of all the devices were analyzed using a Digital Nanoscope III AFM imaging system and analysis software. The surfaces were scanned in contact mode by an atomic force microscope (AFM). The AFM utilized a probe to map the topography and friction of each surface. The AFM was also used to scan the bi-layer structures. Detailed images of active layers were taken with a Bruker Dimension Icon AFM with a conductive tip in PeakForce Tapping mode with ScanAsyst. UV-Vis samples of 4:2:12 PCDTBT:PS:PCBM and 1.2:4:2:12 P3HT:PCDTBT:PS:PCBM were placed into separate glass containers and covered in acetone for 2 hours to selectively dissolve polystyrene.[26] The samples were scanned with the AFM to study the effects of the acetone on the polymer-fullerene blends. A 1:4:2 P3HT:PCDTBT:PS sample was

scanned with a combined Raman-AFM system (Renishaw inVia Confocal Raman Microscope and Bruker Innova AFM) to elucidate the phase separation that occurred.

Results

3.1 UV-Vis Spectra Analysis:

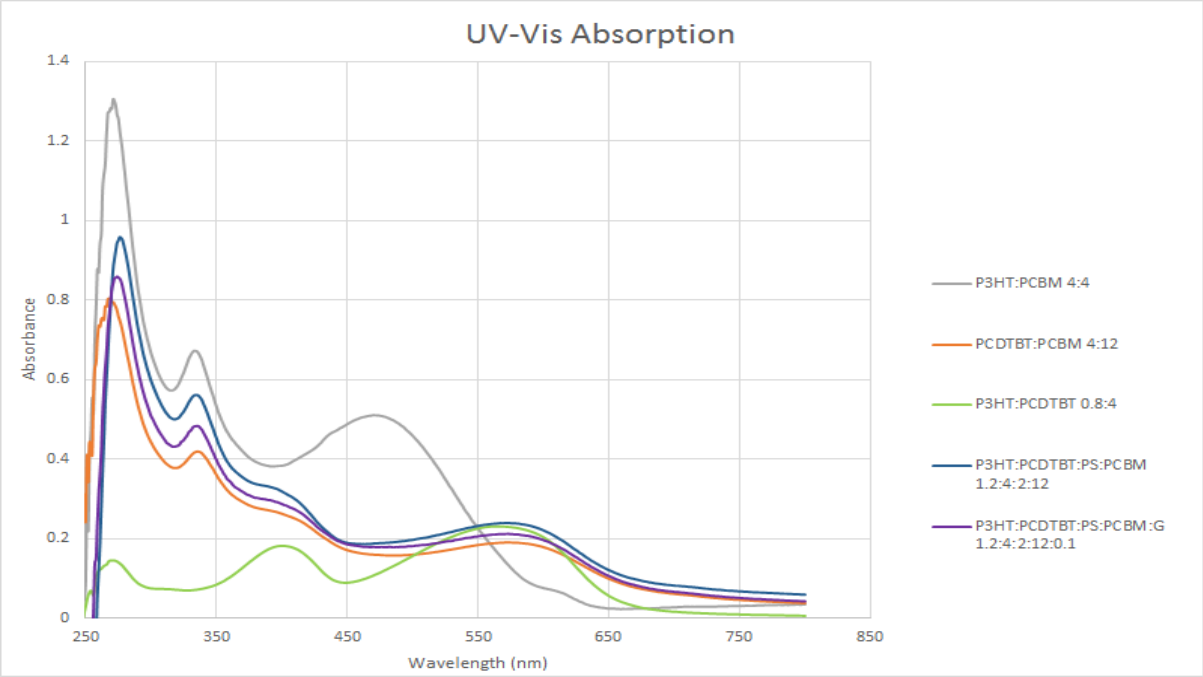

Figure 1. The absorption spectra of various combinations of materials used in the photoactive layers of the solar cells.

Using UV-Vis spectrometry, the absorption spectra of various blends of materials used in the active layer were obtained (Figure 1). The distinct peaks of the photoactive polymers P3HT and PCDTBT can be observed when each is blended with PCBM. The 4:4 P3HT:PCBM absorbance spectrum showed a peak at 470 nm, corresponding to that found in previous literature.[27] Similarly, 4:4 the PCDTBT:PCBM absorbance spectrum showed peaks at 400 nm and 570 nm, in conjunction with a pristine PCDTBT spectrum from literature.[28] The peaks at 270 nm and 333 nm were attributed to PCBM.[27]

The P3HT absorbance peak disappeared when the P3HT was mixed with PCDTBT. The 0.8:4 P3HT:PCDTBT spectrum showed peaks at only 400 nm and 570 nm, indicating the

absorbance of only PCDTBT. This observation suggested that there was an insufficient concentration of P3HT in any one place in the sample to show a noticeable absorption because it was energetically favorable for P3HT to blend into the PCDTBT.

3.2 TEM Analysis:

TEM images revealed that self-assembly occurred in the active layer. The circular shapes showed that columnar structures had formed through phase-segregation of the polymers (Figure 2). The 1.2:4:2:12 P3HT:PCDTBT:PS:PCBM sample (Figure 2a) showed smaller patterned features than the 1.2:4:2:12:0.1 P3HT:PCDTBT:PS:PCBM:Graphene (Figure 2b) sample, indicating that graphene caused an increase in size of the PS domains.

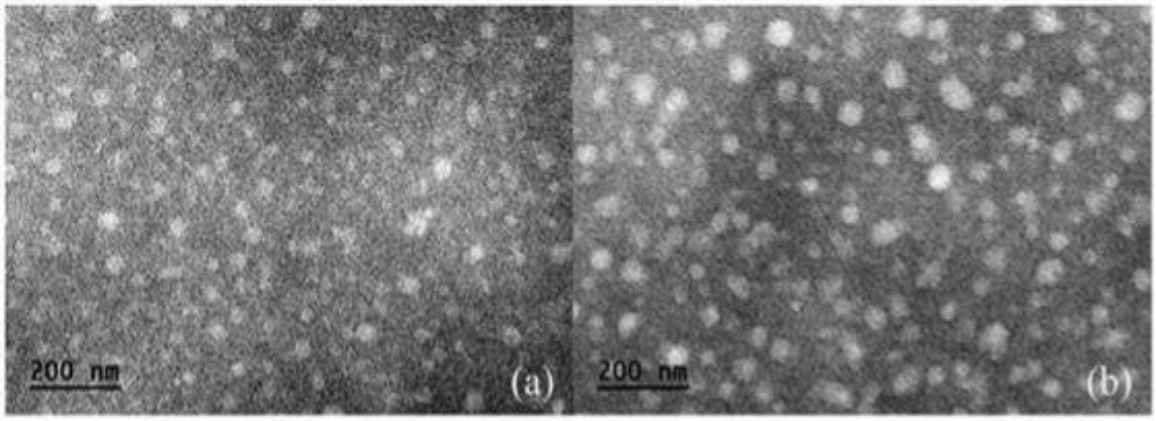

Figure 2. TEM images of (a) 1.2:4:2:12 P3HT:PCDTBT:PS:PCBM and (b) 1.2:4:2:12:0.1 P3HT:PCDTBT:PS:PCBM:Graphene samples.

3.3 AFM Analysis:

Bi-layer structures were made to measure the surface interactions between polymers in the active layer. Interactions between PS and PCDTBT and between P3HT and PCDTBT were investigated. The AFM images were analyzed using Nanoscope software to obtain a contact angle value for each bi-layer film through the average of twenty contact angles taken from each image.

The bi-layer structures made from PS and PCDTBT are shown in Figure 3. The PS thin film on PCDTBT thin film sample had an average contact angle of 20.6° while the PCDTBT thin film on PS thin film sample had an average contact angle of 7.31°. The surface energy of PS has been found to be 40.7 mN/m.[29] Young's equation ($\gamma_{SV} = \gamma_{SL} + \gamma_{LV}\cos\theta$) was then used to calculate for the interfacial energy between PS and PCDTBT.[30]

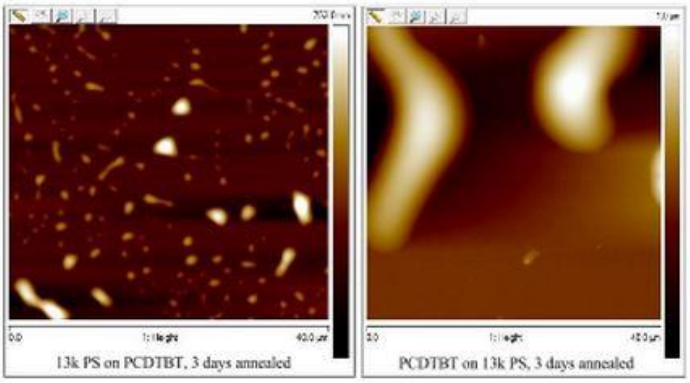

Figure 3. AFM images of the bi-layer structures created with PS of Mw 13k and PCDTBT.

Given: $\gamma_{PS} = 40.7$ mN/m, $\theta_1 = 20.6°$, $\theta_2 = 7.31°$

Equations: (1) $\gamma_{PCDTBT} = \gamma_{PS/PCDTBT} + \gamma_{PS}\cos\theta_1$; (2) $\gamma_{PS} = \gamma_{PS/PCDTBT} + \gamma_{PCDTBT}\cos\theta_2$

Solving for γ_{PCDTBT}: $\gamma_{PS} - \gamma_{PCDTBT} = \gamma_{PCDTBT}\cos\theta_2 - \gamma_{PS}\cos\theta_1$

$$\gamma_{PS}(1 + \cos\theta_1) = \gamma_{PCDTBT}(1+\cos\theta_2)$$

$$\gamma_{PCDTBT} = \frac{1 + \cos\theta 1}{1+\cos\theta 2}\gamma_{PS} = \frac{1 + \cos(20.6°)}{1+\cos(7.31°)}(40.7 \text{ mN/m}) = 39.6 \text{ mN/m}$$

Thus, $\gamma_{PS/PCDTBT} = \gamma_{PCDTBT} - \gamma_{PS}\cos\theta_1 = 39.6 - 40.7\cos(20.6°) = 1.46$ mN/m.

For the bi-layer thin films made from P3HT and PCDTBT (Figure 4), the P3HT thin film on PCDTBT thin film sample had an average contact angle of 2.42° while the PCDTBT thin film on P3HT thin film sample had an average contact angle of 2.30°. The surface energy of P3HT was found to be 27.0 mN/m.[31] The interface energy between PS and PCDTBT was then calculated.

Given: $\gamma_{P3HT} = 27.0$ mN/m, $\theta_1 = 2.42°$, $\theta_2 = 2.30°$

Equations: (1) $\gamma_{PCDTBT} = \gamma_{P3HT/PCDTBT} + \gamma_{P3HT}\cos\theta_1$; (2) $\gamma_{P3HT} = \gamma_{P3HT/PCDTBT} + \gamma_{PCDTBT}\cos\theta_2$

Solving for γ_{PCDTBT}: $\gamma_{P3HT} - \gamma_{PCDTBT} = \gamma_{PCDTBT}\cos\theta_2 - \gamma_{P3HT}\cos\theta_1$

$$\gamma_{P3HT}(1 + \cos\theta_1) = \gamma_{PCDTBT}(1+\cos\theta_2)$$

$$\gamma_{PCDTBT} = \frac{1+\cos\theta 1}{1+\cos\theta 2}\,\gamma_{P3HT} = \frac{1+\cos(2.42°)}{1+\cos(2.30°)}\,(27.0\ mN/m) = 27.0\ mN/m$$

Thus, $\gamma_{P3HT/PCDTBT} = \gamma_{PCDTBT} - \gamma_{P3HT}\cos\theta_1 = 27.0 - 27.0\cos(2.42°) = 0.023$ mN/m.

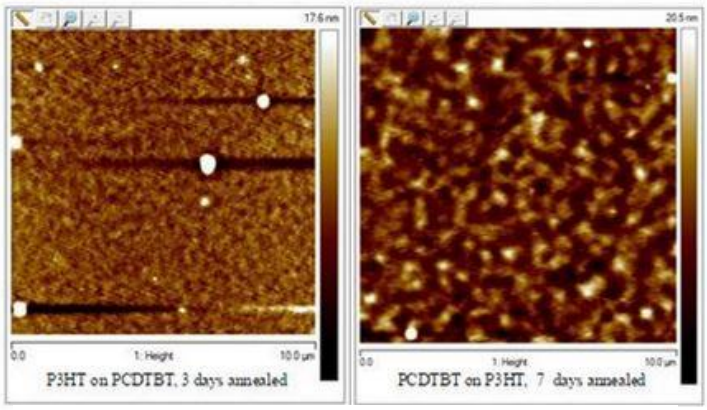

Figure 4. AFM images of the bi-layer structures created with P3HT and PCDTBT.

As $\gamma_{P3HT/PCDTBT}$ is smaller than $\gamma_{PS/PCDTBT}$, PCDTBT is shown to be more compatible with P3HT. The surface energy calculations confirmed that PCDTBT and PS interacted poorly, causing two polymers to phase-separate and form nanostructures. In addition, as the surface tension between P3HT and PCDTBT was so small, these two polymers combined together in the active layer and did not show detectable phase separation.

The acetone-etched samples had PS removed from their systems. The absence of PS can been seen in the circular holes present in their AFM images (Figure 5). The domain sizes for the 4:2:12 PCDTBT:PS:PCBM sample were noticeably smaller than that of the 1.2:4:2:12 P3HT:PCDTBT:PS:PCBM sample, indicating that P3HT caused the PCDTBT and PS to phase-separate to a greater degree.

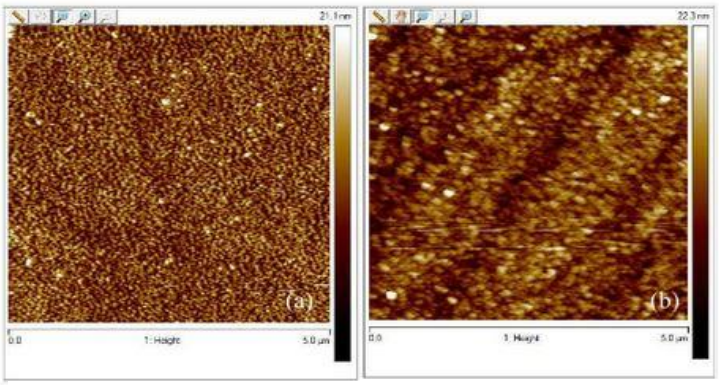

Figure 5. AFM images of (a) 4:2:12 PCDTBT:PS:PCBM and (b) 1.2:4:2:12 P3HT:PCDTBT:PS:PCBM samples washed in acetone to

The combined Raman-AFM scan (Figure 6) shows the chemical profiles of the polymer blend. The Raman spectra of three polymers used in the active layer are shown, and the composite image reveals how the polymers have organized. The P3HT is shown to aggregate near the PS while the PCDTBT is seen to gather

away from the PS. A relatively large amount of PCDTBT is seen, as expected from the polymer ratios.

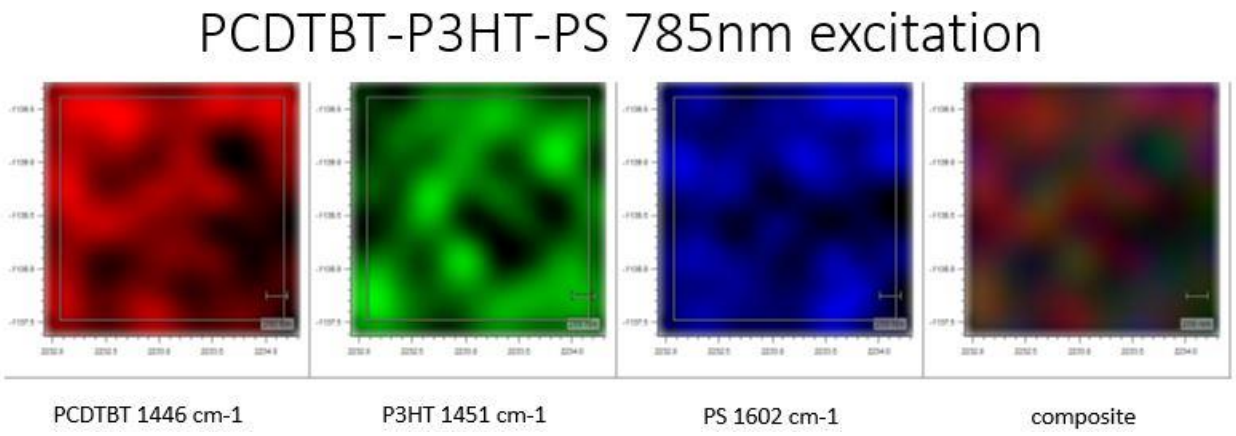

Figure 6. The Raman-AFM scans of the 1:4:2 P3HT:PCDTBT:PS sample are shown. The distinct Raman profiles of each polymer is illustrated, as well as the composite of all Raman spectra.

AFM images were taken of the active layers of the devices (Figure 7). The nanoscale columnar structures, expected to appear as circular shapes when scanned from above, were difficult to distinguish. All features of self-assembly were sub-micron and thus could not be imaged clearly at this scale. The topography was relatively smooth for all the devices. Figure 7f shows that the conductance of the active layer is roughly the same throughout, indicating that a thin layer of PCBM covered the top of the active layer.

Component	Ratio (mg/mL)	Spin Speed (rpm)	Average Contact Angle (°)	Average Arithmetic Roughness (nm)
PCDTBT:PS:PCBM	4:2:12	2000	1.933	0.536
P3HT:PCDTBT:PS:PCBM	0.5:4:2:12	2000	0.915	0.518
P3HT:PCDTBT:PS:PCBM	1:4:2:12	2000	1.257	0.579
P3HT:PCDTBT:PS:PCBM	0.8:4:2:12	2000	1.347	0.755
P3HT:PCDTBT:PS:PCBM	1.2:4:2:12	2000	1.625	0.625
P3HT:PCDTBT:PS:PCBM:G	1.2:4:2:12:0.1	2000	1.592	0.520

Table 1. The average contact angle and roughness were obtained for select devices through analysis of their AFM images. Twenty values of contact angle and roughness were obtained from each image to calculate the average values.

To analyze the molecular interactions within the active layers, average contact angle and roughness values were obtained from the AFM images (Table 1). Devices with greater amounts of P3HT showed higher contact angles on average, indicating that the active layers had become more hydrophobic. For the devices with only P3HT as the additive, increasing roughness correlated with increasing efficiency. These trends indicated that the P3HT aggregated at the interfaces between PS and PCDTBT. When more P3HT was present at the interface, the device was more efficient, confirmed by the high-performing 0.8:4:2:12 P3HT:PCDTBT:PS:PCBM device, which had the highest roughness of 0.755 nm.

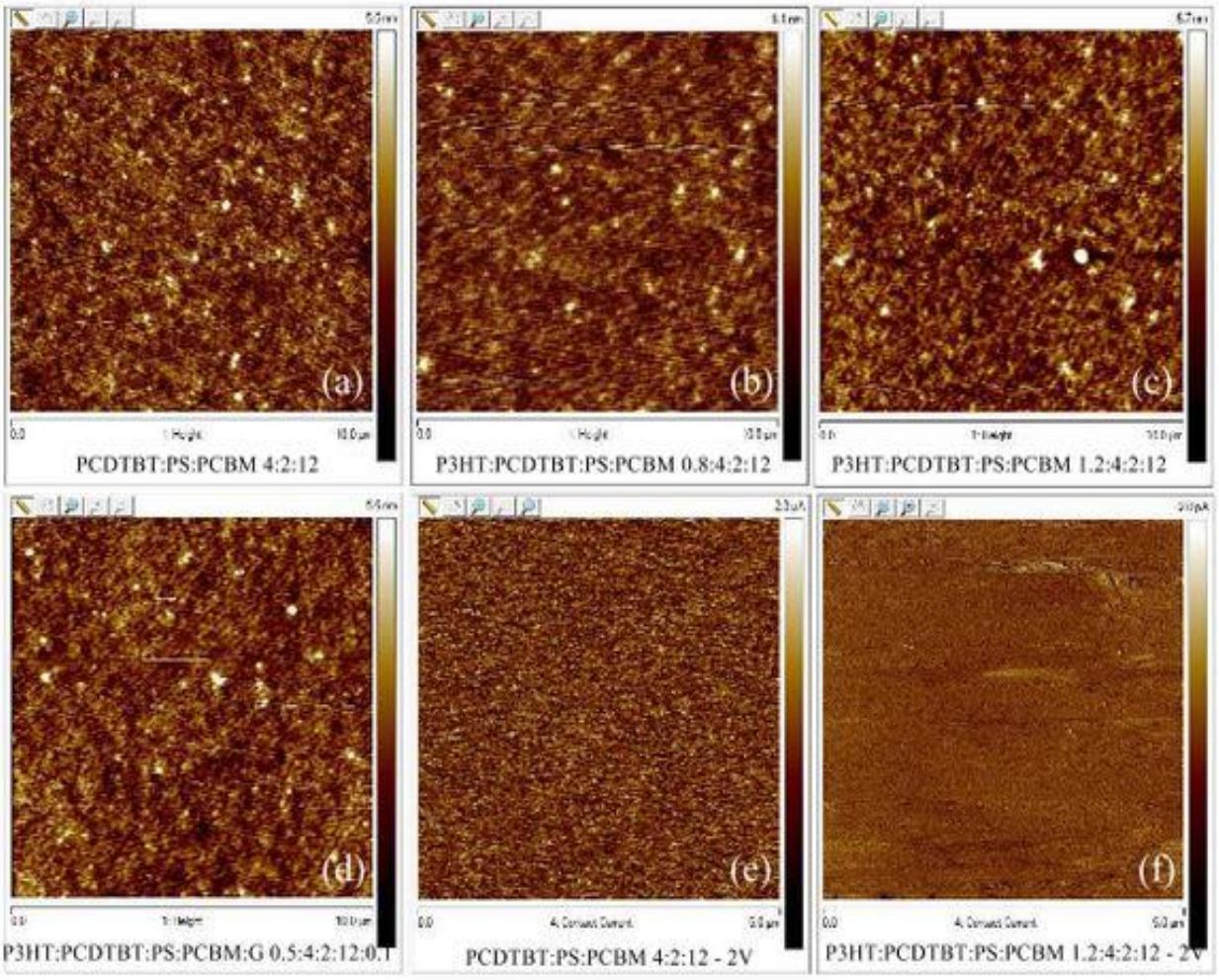

Figure 7. The active layers of various solar cells were imaged with an AFM in contact mode (a-d) and an AFM with a conductive tip (e,f).

The AFM data also showed that graphene had a noticeable effect on the morphology of the active layer. The 1.2:4:2:12 P3HT:PCDTBT:PS:PCBM device had a contact angle of 1.625° and roughness of 0.625 nm while the 1.2:4:2:12:0.1 P3HT:PCDTBT:PS:PCBM:Graphene device had a contact angle of 1.592° and a roughness of 0.520 nm. The decrease in contact angle and roughness with the addition of graphene indicated that graphene was present at the interfaces of the columnar structures, and it helped compatibilize the photoactive polymers and PCBM.

3.4 Device Performance:

Component	Ratio (mg/mL)	Spin Speed (rpm)	Voc (V)	Jsc (mA/cm^2)	FF	PCE (%)
PCDTBT:PS:PCBM (control)	4:2:12	2000 rpm	0.732	6.01	0.476	2.10
P3HT:PCDTBT:PS:PCBM	0.5:4:2:12	2000 rpm	0.730	5.20	0.441	1.67
P3HT:PCDTBT:PS:PCBM	0.5:4:2:12	3000 rpm	0.773	5.04	0.450	1.75
P3HT:PCDTBT:PS:PCBM	1:4:2:12	2000rpm	0.800	5.75	0.401	1.87
P3HT:PCDTBT:PS:PCBM	1:4:2:12	3000 rpm	0.735	5.55	0.394	1.61
P3HT:PCDTBT:PS:PCBM	0.8:4:2:12	2000rpm	0.810	7.39	0.394	2.36
P3HT:PCDTBT:PS:PCBM	0.8:4:2:8	2000rpm	0.623	5.92	0.368	1.35
P3HT:PCDTBT:PS:PCBM	1.2:4:2:12	2000rpm	0.723	6.26	0.360	1.65
P3HT:PCDTBT:PS:PCBM:G	1.2:4:2:12:0.1	2000rpm	0.830	7.53	0.516	3.22

Table 2. Several photovoltaic parameters were obtained for each device. All values shown here are averaged from the four trials tested for every device.

The performance of each device was measured through the photovoltaic parameters of open circuit voltage (V_{OC}), short circuit current (J_{SC}), fill factor (FF), and power conversion efficiency (PCE). The J_{SC} showed the relative spectrum of light absorbed by each device. The 0.8:4:2:12 P3HT:PCDTBT:PS:PCBM device had a J_{SC} of 7.39, a statistically significant increase over the control device J_{SC} of 6.01 ($p = 0.003$). The device with graphene had the highest J_{SC} of

7.53, also statistically different from that of the control cell ($p = 0.0002$). The significant increase in J_{SC} indicated that P3HT was absorbing light and had expanded the spectral range of the cell.

Power conversion efficiency was used to compare the device performance of one solar cell to another. The standard Students one tailed t-test was used to calculate statistical significance of the difference in efficiency between the cells using the individual values obtained from each trial of the devices. Comparing the cells with various ratios of P3HT, the 0.8:4:2:12 P3HT:PCDTBT:PS:PCBM device had the highest efficiency of 2.36%, showing a 12.4% increase over the control device without P3HT, which had a PCE of 2.10%. This increase was statistically significant ($p = 0.0001$), verifying that the addition of a 0.8 wt. ratio of P3HT improved device performance. The other devices with P3HT decreased in efficiency when compared to the control cell, due to morphology changes with the addition of the second electron donor. A significant increase in efficiency was observed when graphene was incorporated into the active layer. The 1.2:4:2:12:0.1 P3HT:PCDTBT:PS:PCBM:Graphene device showed the highest efficiency of 3.22%, a 95.2% increase over the 1.2:4:2:12 P3HT:PCDTBT:PS:PCBM device without graphene, with a PCE of 1.65%. This statistically significant increase in device performance ($p = 0.0002$) was attributed the ability of the graphene to integrate the various components in the active layer.

Discussion

The addition of P3HT and graphene increased the efficiency of the organic solar cells, as hypothesized, and these materials were shown to have significant effects on the morphology of the active layer as well. The addition of a 0.8 wt. ratio of P3HT led to improved solar cell efficiency. The statistically significant increase in J_{SC} when P3HT was added demonstrated that the absorption spectrum of the device was expanded, and more light was absorbed by the device. This study is the first to describe the effect of a second electron donor on ordered organic photovoltaics. The

increase in contact angle and roughness of the active layers revealed that the P3HT diffused toward the sides of the self-assembled columnar structures (Figure 8). The second photoactive polymer did not, however, have much contact with the PCBM, as the addition of P3HT into the devices increased efficiency by a limited amount. This work is the first to integrate of multiple donors into a self-assembled organic solar cell. Similar surface energies indicate miscibility,[32] so the small calculated interfacial energy between P3HT and PCDTBT suggested that the two polymer phases would combine partially with each other.

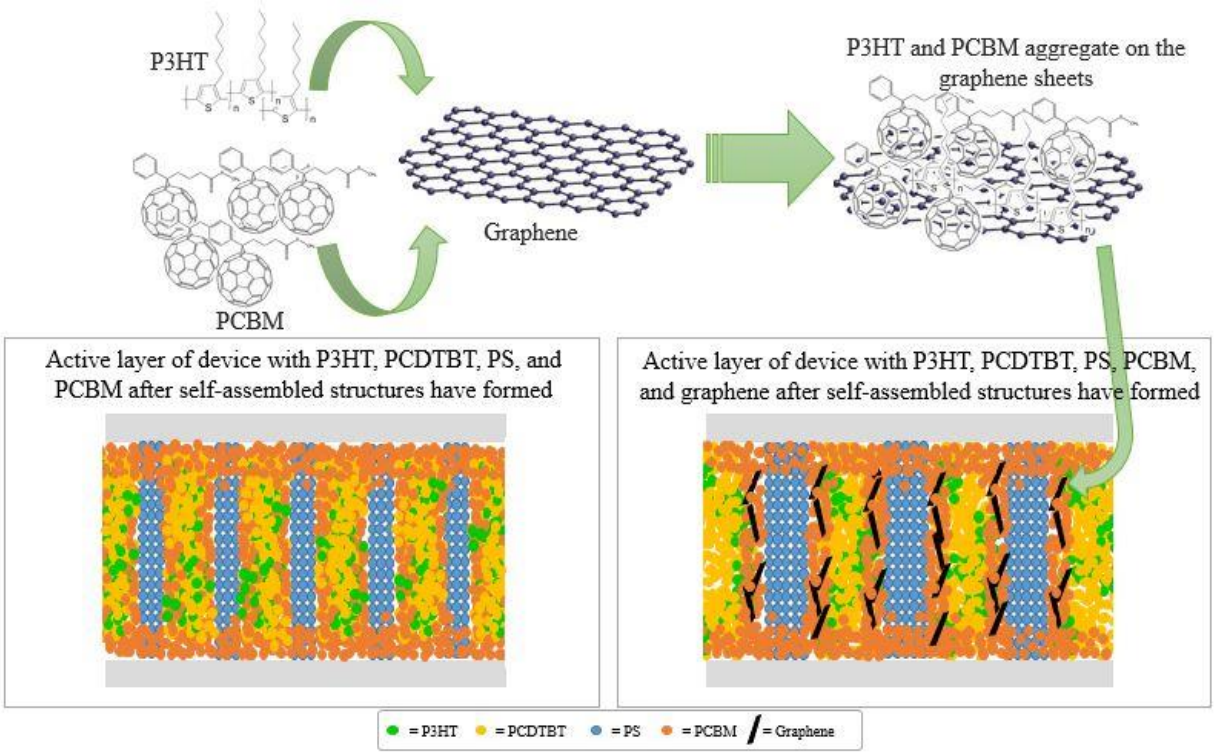

Figure 8. Models of cross-sections of the active layers are shown. Graphene induced the diffusion of P3HT and PCBM towards the interfaces of the columnar structures.

Solar cell efficiency was substantially increased with the incorporation of a small fraction graphene. This research showed that graphene functioned as more than just an electron transport material, since it also had a considerable impact on the morphology of the active layer. Graphene aggregated at the sides of the columnar structures, where the interfaces between the donor and acceptor materials were present (Figure 8), as shown by the lowered contact angle and roughness

of the active layer when graphene was added. PCBM was induced to diffuse towards the graphene, as PCBM has been shown to be attracted to areas of high surface energy.[23] The fullerene material was able to spread more continuously along the nanoscale columns, maximizing contact with the electron donors so that more electricity was generated. The highest J_{SC} was observed in the device with graphene, indicating that the P3HT was also drawn to the interfaces by graphene. The photoresponse of the solar cells was expanded as greater amounts of P3HT were able to make contact with the electron acceptors to generate electrical energy. As Figure 8 shows, graphene filled in areas along the nanostructures lacking PCBM and helped gather the P3HT to the interfaces, resulting in the significant increase in device efficiency. These findings are consistent with past research showing that graphene acts as an electron acceptor material to improve cell efficiency,[15] but this project describes the specific morphological effects of graphene in the nanostructured active layer.

After an extensive literature review, no previous work has been found on incorporating additives into nano-architectured active layers of organic solar cells. To the best of my knowledge, this research is the first time the effect of a secondary electron donor and graphene on the morphology of a self-assembled active layer has been studied. Though the efficiency of the devices were low compared to those obtained in current research, the relative increase over the control device shows that the addition of P3HT and graphene help device performance significantly. This work presents a very economical way of increasing device performance, as only minute additions of P3HT and graphene were needed for significant increases in efficiency.

Conclusions

This research explored the effects of the combination of two photoactive polymers and graphene on the efficiency and morphology of a self-assembled heterojunction solar cell system.

Polymer interactions were found to be critical in device performance, and graphene acted as a binding agent to help compatibilize the various components in the photoactive layers. The hypothesis that the incorporation of an additional electron donor and graphene into these solar cells would improve their efficiencies was proven true.

The interactions between the various components within the active layer were shown to be complex, and morphology had a large impact on device performance. The AFM analysis as well as the UV-Vis spectroscopy showed that the photoactive polymers PCDTBT and P3HT blended with each other to a certain degree. PCDTBT phase-segregated differently with PS when P3HT was added, resulting in decreased device performance in some solar cells. Graphene was shown to help both P3HT and PCBM aggregate at the interfaces of the PS columnar structures, leading to a substantial increase in cell efficiency.

In the future, I would like to find the optimal ratios of the P3HT and graphene for these devices. Confocal microscopy will be used to confirm the organization of the electron donors and acceptors. TEM will be attempted on cross-sections of the active layers to obtain better images of the columnar structures. Additional research includes investigating how another immiscible polymer would influence the morphology and device performance of this active layer system. A polymer that is more hydrophilic and less absorptive, such as Poly(methyl methacrylate) (PMMA), could increase self-assembly within the system by decreasing domain size and prevent the two photoactive polymers from combining. PMMA also has a higher surface energy than PS, so it could increase preferential segregation of PCBM on the nanostructures. With continued research on the incorporation of multiple donors and acceptors into self-assembled organic solar cells, these devices will integral in renewable energy.

References

1. The Energy Crisis and Climate Change. Finding Solutions. Together. (2009). *Global Economic Synopsium.*
2. Power in Our Hands: Renewable Energy & Fossil Fuels in the United States. (2011). IndyKids!
3. Harvey, F. (2015). World Only Half Way to Meeting Emissions Target with Current Pledges. *The Guardian*.
4. Scharber, M.C., & Sariciftci N.S. (2013). Efficiency of bulk-heterojunction organic solar cells. *Progress in Polymer Science, 38*(12), 1929-1940.
5. Li, G., Yang, Y., & Zhu, R. (2012). Polymer solar cells. *Nature Photonics, 6*, 153-161.
6. Hoppe, H., & Sariciftci, N. S. (2004). Organic solar cells: An overview. *Journal of Materials Research, 19*(7), 1924-1945.
7. Pan, C., Li, H., Akgun, B., Satijia, S. K., Zhu, Y., Xu, D., Ortiz, J., Gersappe, D., & Rafailovich, M. H. (2013). Enhancing the Efficiency of Bulk Heterojunction Solar Cells via Templated Self-Assembly. *Macromolecules, 46*(5), 1812–1819.
8. Ameri, T., Khoram, P., Min, J., & Brabec, C. J. (2013). Organic Ternary Solar Cells: A Review. *Advanced Materials, 25*(31), 4245–4266.
9. Blouin, N., Michaud, A., & Leclerc, M. (2007). A Low-Bandgap Poly(2,7-Carbazole) Derivative for Use in High-Performance Solar Cells. *Advanced Materials, 19*(17), 2295–2300.
10. Wang, D., Kim, J. K., Seo, J. H., Park, O. O., & Park, J. K. (2012). Stability comparison: A PCDTBT/PC71BM bulk-heterojunction versus a P3HT/PC71BM bulk-heterojunction. *Solar Energy Materials and Solar Cells, 101*, 249-255.
11. Peters, C. H., Sachs-Quintana, I. T., Kastrop, J. P., Beaupré, S., Leclerc, M. & McGehee, M. D. (2011). High Efficiency Polymer Solar Cells with Long Operating Lifetimes. *Advanced Energy Materials, 1*(4), 491–494.
12. Zhu, X., An, Q., Huang, H., Jiao, C., & Zhang F. (2015). Improved efficiency of ternary the blend polymer solar cells by doping a narrow band gap polymer material. *Science China Physics, Mechanics & Astronomy, 58*(3), 037001.
13. Machui, F., Rathgeber, S., Li, N., Ameri, T., & Brabec, C. J. (2012). Influence of a ternary donor material on the morphology of a P3HT:PCBM blend for organic photovoltaic devices. *Journals of Materials Chemistry, 22*(31), 15570-15577.
14. Gupta, V., Bharti, V., Kumar, M., Chand, S., & Heeger, A. J. (2015). Polymer–Polymer Förster Resonance Energy Transfer Significantly Boosts the Power Conversion Efficiency of Bulk-Heterojunction Solar Cells. *Advanced Materials, 27*(30) 4398–4404.
15. Iwan, A., & Chuchmała, A. Perspectives of applied graphene: Polymer solar cells. *Progress in Polymer Science, 37*(12), 1805-1828.
16. Wang, H., He, D., Wang, Y., Liu, Z., Wu, H., & W., J (2011). Organic photovoltaic devices based on graphene as an electron-acceptor material and P3OT as a donor material. *physica status solidi (a), 208*(10), 2339-2343.
17. Liu, Q., Liu, Z., Zhang, X., Zhang, N., Yang, L., Yin, S., & Chen Y. (2008). Organic photovoltaic cells based on an acceptor of soluble graphene. *Applied Physics Letters, 92*(22), 223303.

18. Robaeys, P., Bonaccorso, F., Bourgeois, E., D'Haen, J., Dierckx, W., Dexters, W., Spoltore, D., Drijkoningen, J., Liesenborgs, J., Lombardo, A., Ferrari, A. C., Reeth, F. V., Haenen, K., Manca, J. V., & Nesladek, M. (2014). Enhanced performance of polymer:fullerene bulk heterojunction solar cells upon graphene addition. *Applied Physics Letters, 105*(8), 083306.
19. Liu, Z., He, D., Wang, Y., Wu, H., & Wang, J. (2010). Graphene doping of P3HT:PCBM photovoltaic devices. *Synthetic Metals, 160*(9–10), 1036-1039.
20. Liu, Q., Liu, Z., Zhang, X., Yang, L., Zhang, N., Pan, G., Yin, S., Chen, Y., & Wei, J. (2009). Polymer Photovoltaic Cells Based on Solution-Processable Graphene and P3HT. *Advanced Functional Materials, 19*(6), 894–904.
21. Ye, L., Xiao, T., Zhao, N., Xu, H., Xiao, Y., Xu, J., Xiong, Y., & Xu, W. (2012). Derivitization of pristine graphene for bulk heterojunction polymeric photovoltaic devices. *Journals of Material Chemistry, 22*(33), 16723.
22. Yu, F., & Kuppa, V. K. (2013). Enhancement in the performance of organic photovoltaic devices with pristine graphene. *Materials Letters, 99*, 72-75.
23. Das, S., Sudhagar, P., Kang, Y. S., & Choi, W. (2013). Graphene synthesis and application for solar cells. *Journal of Materials Research, 29*(3), 299-319.
24. Wan, X., Long, G., Huang, L., & Chen, Y. (2011). Graphene – A Promising Material for Organic Photovoltaic Cells. *Advanced Materials, 23*(45), 5342-5358.
25. Tao, C., Ruan, S., Zhang, X., Xie, G., Shen, L., Kong, X., Dong, W., Liu, C., & Chen, W. (2008). Performance improvement of inverted polymer solar cells with different top electrodes by introducing a MoO_3 buffer layer. *Applied Physics Letters, 93*(19), 193307.
26. Xue, H., Kong, X., Liu, Z., Liu, C., Zhou, J., Chen, W., & Xu, Q. (2007). TiO2 based metal-semiconductor-metal ultraviolet photodetectors. *Applied Physics Letters, 90*(20), 201118.
27. Turkovic, V., Engmann, S., Egbe, D. A.M., Himmerlich, M., Krischok, S., Gobsch, G., & Hoppe, H. (2013). Multiple stress degradation analysis of the active layer in organic photovoltaics. *Solar Energy Materials & Solar Cells, 120,* 654-668.
28. Chow, T. S. (1998). Wetting of rough surfaces. *Journal of Physics: Condensed Matter, 10,* L445-L451.
29. Vohra,V., Campoy-Quiles, M., Garriga, M., & Murata, H. (2012). Organic solar cells based on nanoporous P3HT obtained from self-assembled P3HT:PS templates. *Journals of Materials Chemistry, 22*(37), 20017.
30. Nalwa, H. S. (2002). *Handbook of Thin Film Materials.* London: Academic Press.
31. Jung, B., Kim, K., & Kim, W. (2014). Microwave-assisted solvent vapor annealing to rapidly achieve enhanced performance of organic photovoltaics. *Journal of Materials Chemistry A, 2*(36), 15175-15180.
32. Khlyabich, P. P., Rudenko, A. E., Street, R. A., & Thompson, B. C. (2014). Influence of Polymer Compatibility on the Open-Circuit Voltage in Ternary Blend Bulk Heterojunction Solar Cells. *ACS Applied Materials & Interfaces, 6*(13), 9913-9919.